Supporting Information: Optical Generation and Detection of Local Nonequilibrium Phonons in Suspended Graphene

Sean Sullivan,[1] Ajit Vallabhaneni,[2] Iskandar Kholmanov,[3] Xiulin Ruan,[2] Jayathi Murthy,[4] Li Shi[1,3]*

[1]Materials Science and Engineering Program, [3]Department of Mechanical Engineering, University of Texas at Austin, Austin, Texas 78712

[2]School of Mechanical Engineering, Purdue University, West Lafayette, Indiana 47907

[4]Department of Mechanical and Aerospace Engineering, University of California, Los Angeles, California 90095

*Email: lishi@mail.utexas.edu

Contents

1. All measured Stokes band positions

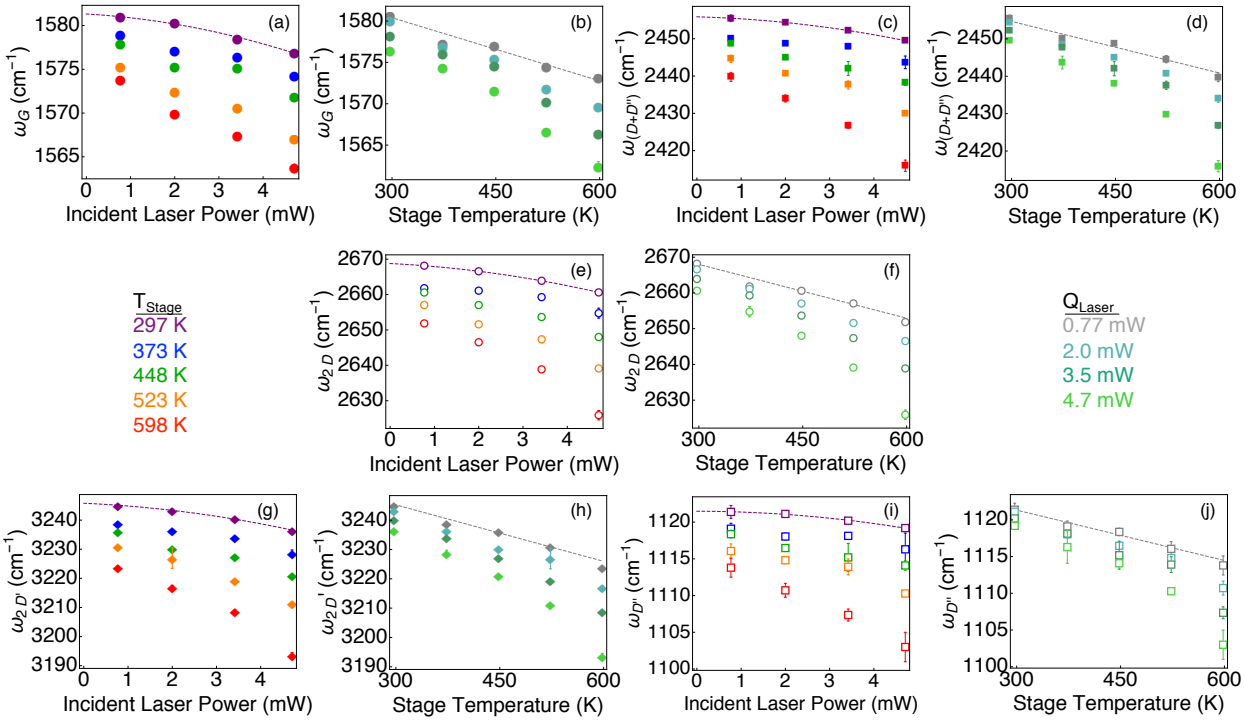

Figure S1: The measured Stokes shift values as function of incident laser power and stage temperature for the G-band (a, b), (D+D'')-band (c, d), 2D-band (e, f), 2D'-band (g, h), and the D'' frequencies (i, j). The D'' frequencies were extracted from the 2D and (D+D'')-bands.

2. All measured phonon temperatures

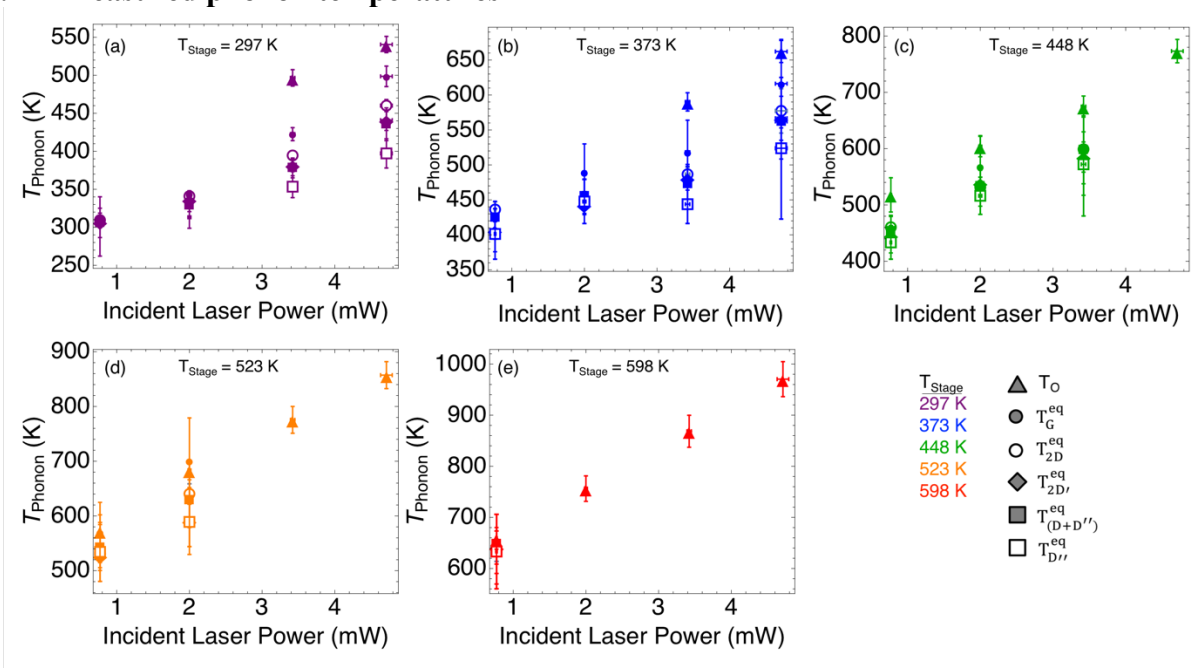

Figure S2: All of the measured phonon temperature values taken from different peak shifts and intensity ratios with increasing stage temperature from 297 K to 598 K from (a) to (e). The measured nonequilibrium is more apparent at lower stage temperatures and higher laser powers, and becomes comparable to the measurement uncertainties as either the stage temperature is increased or the laser power is reduced. Peak shift-predicted temperature data are not shown for the highest laser power.

3. Multi-temperature model

In order to better understand the observed local nonequilibrium among the different phonon polarizations, we have calculated the energy carrier temperatures in suspended graphene under the experimental conditions. As described in detail in a recent publication,[1] we first use density functional perturbation theory to directly calculate the electron-phonon scattering rates in graphene. Based on these rates, we utilize a multi-temperature model to compute the temperatures of the electrons and six phonon polarizations as energy is transferred from the incident photons to the graphene electrons and optical phonons, and to the lower energy polarizations at different rates. Based on this calculation, we find that the electrons and the

optical phonons may be driven significantly out of local equilibrium from the acoustic phonons and the out-of-plane polarized transverse acoustic (ZA) modes, in particular.

Figures S3 and Figure S4 shows the calculation results for the case of 0.77 mW incident laser power, a stage temperature (T_{Stage}) of 297 K, a Gaussian beam radius of 360 nm, and optical absorption of 3.1%. The calculations were carried out in a 5x5 μm^2 Cartesian domain with quarter symmetry, which is equivalent to the experimental case of graphene suspended over a 10 μm-diameter hole as the calculated temperature rise at a distance of 5 μm from the center is negligible. Because past measurements have yielded much lower electronic thermal conductivity values than the intrinsic value calculated from first principles due to the presence of impurities and defects in the measured samples,[1] different electronic thermal conductivity values have been used in the calculation. In Fig. S4 an electronic thermal conductivity of $\kappa_e = (20\ \mathrm{W}m^{-1}K^{-1})\ T_e/300\ K$ is assumed. Calculations with other electronic thermal conductivities were performed, and the effects on the nonequilibrium between energy carriers were found to be small, as summarized in Table S1, which presents the average temperature inside the Gaussian laser spot.[1] The reason is that the thermal conductivity contribution from the hot electrons is much smaller than the thermal conductivity contributions from phonons in the laser spot. Consequently, the electron heat current becomes considerably smaller than the phonon heat current outside the Gaussian radius, despite the still higher electron temperature than the phonon temperatures, as shown in Fig. S5. In particular, ZA phonons are found to be the largest contributor to the heat current, despite the lowest temperature rise. This result reflects the large specific heat and thermal conductivity contribution from the ZA phonons in the temperature range.

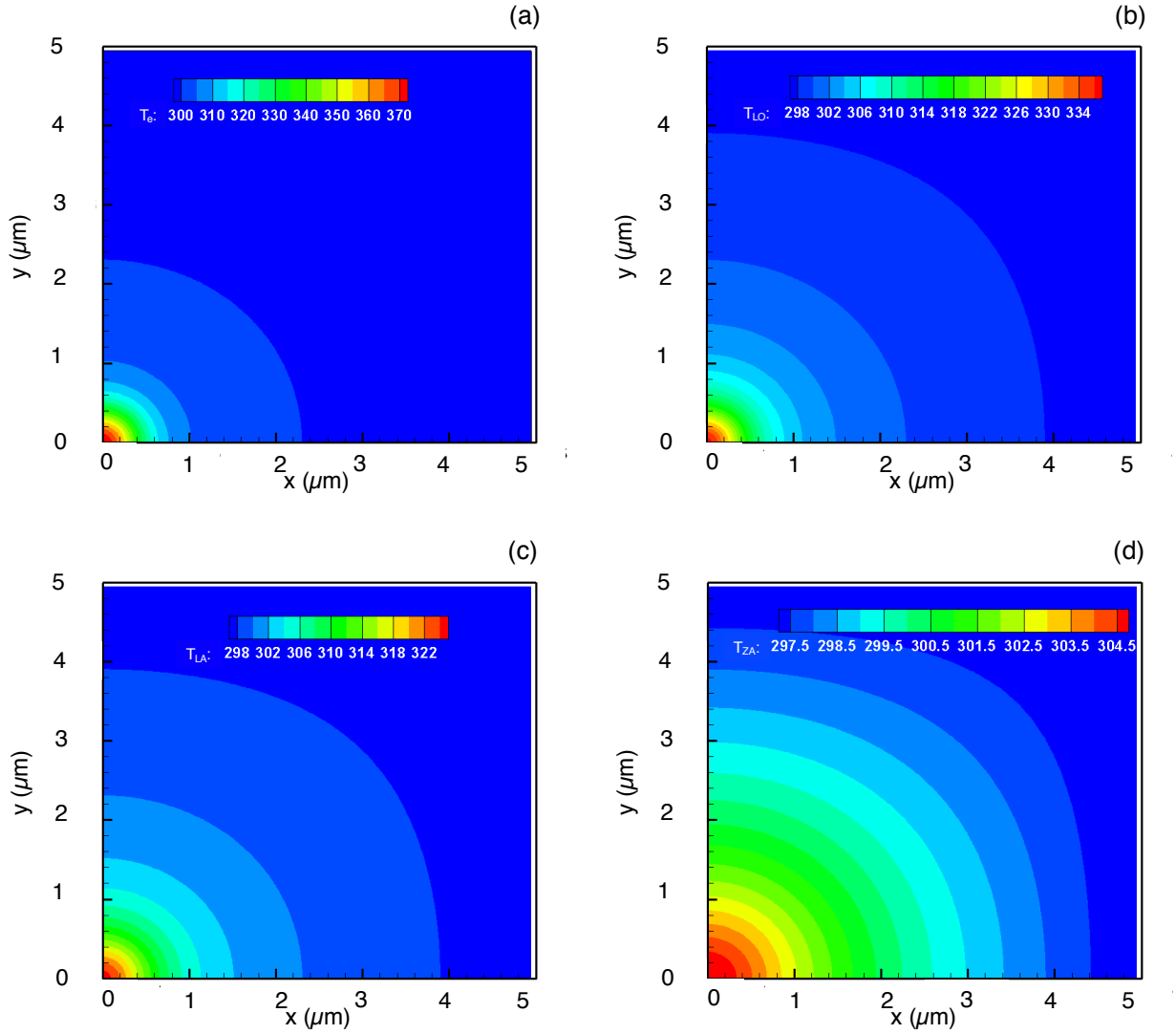

Figure S3: Calculated (a) electronic, (b) longitudinal optical (LO), (c) longitudinal acoustic (LA), and (d) out-of-plane polarized transverse acoustic (ZA) temperatures in graphene suspended over a 10 µm x 10 µm hole for the conditions of 0.77 mW incident laser power, T_{Stage} = 297 K, a beam radius of 360 nm, and laser absorption of 3.1%. The electronic thermal conductivity in this simulation was assumed to follow $(20\ \mathrm{W}m^{-1}K^{-1})\,T_e/300\ K$.

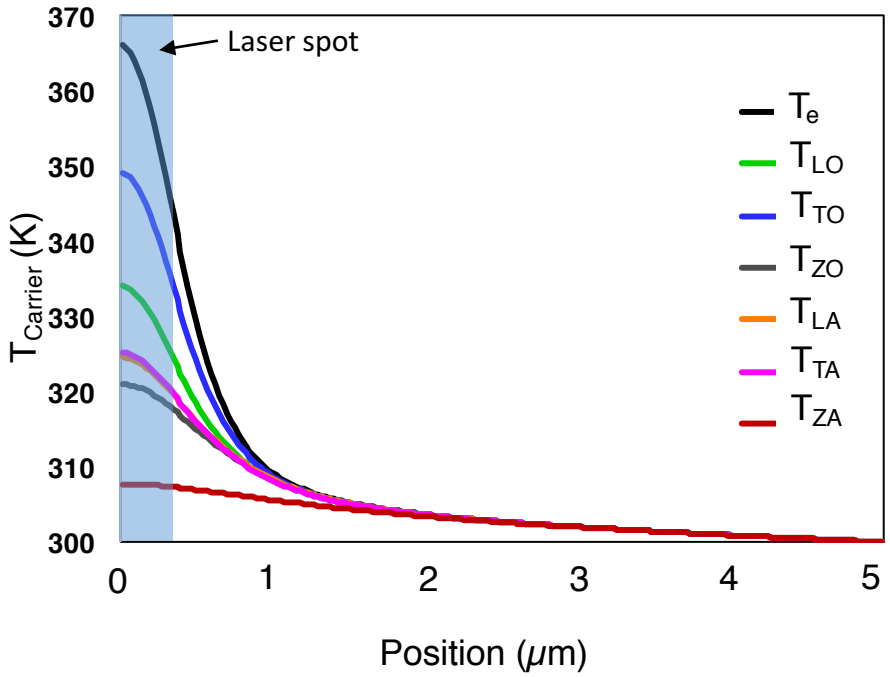

Figure S4: Temperature profiles along the x-axis for the electrons, six phonon polarizations based on the multi-temperature model and first-principles-derived electron-phonon relaxation times for the conditions of 0.77 mW incident laser power and T_{Stage} = 297 K. The electronic thermal conductivity in this calculation was assumed to follow $(50\ \mathrm{W}m^{-1}K^{-1})\ T_e/300\ K$.

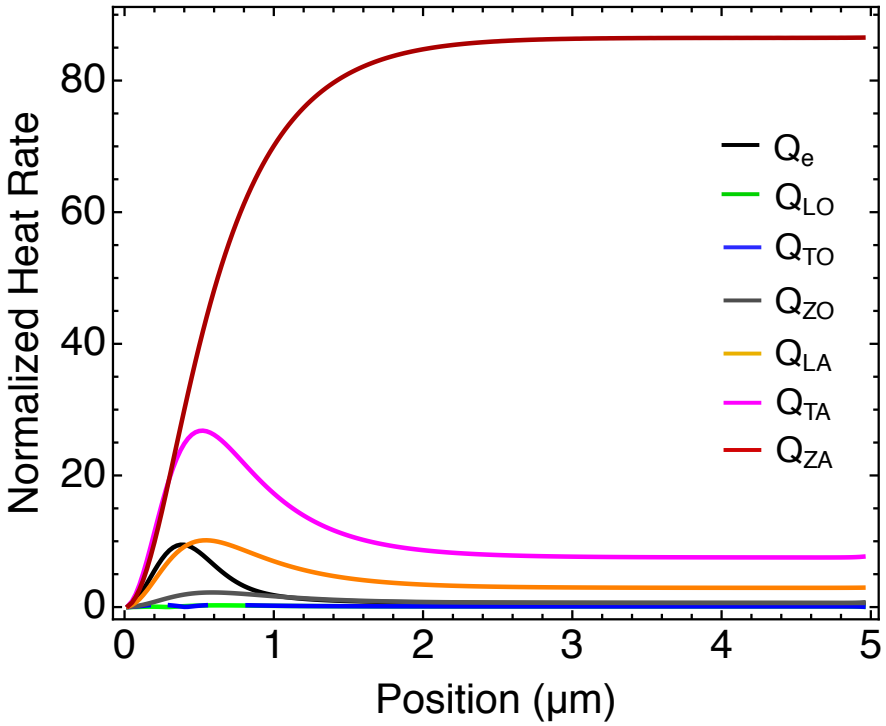

Figure S5: Calculated contributions from different energy carriers to the heat transfer rate across a square domain that is concentric with the laser spot as a function of x-position of the right edge of the square. The heat rate contribution is normalized to the total input heat rate from the laser. The incident laser power is 0.77 mW and the stage temperature is 297 K. For this calculation, the electronic thermal conductivity was assumed to equal $(20\ \mathrm{W}m^{-1}K^{-1})\,T_e/300\ K$.

The effects of stage temperature and laser power on the local nonequilibrium are shown in Table S1. The largest nonequilibrium is predicted between the electronic temperature and the ZA phonon temperature. Additionally, the simulations indicate that even at the lowest laser power of 0.77 mW, the ZA phonons are still underpopulated with respect to higher-energy phonon polarizations and electrons, as indicated in Table S2, which shows the ratio of the ZA temperature rise relative to the temperature rise of other energy carriers. A smaller ratio reflects a larger nonequilibrium between the ZA phonons and the other carriers. In addition, the prior calculation shows that these ratios are very small even when the laser power decreases to as low as 0.01 mW, suggesting pronounced local nonequilibrium at the low laser power. [1]

Table S1: Calculated Average Energy Carrier Temperatures in the Laser Spot at Different Laser Powers, Stage Temperatures, and Electronic Thermal Conductivities

κ_e ($Wm^{-1}K^{-1}$)	Power (mW)	T_{stage} (K)	T_e	T_{LO}	T_{TO}	T_{zo}	T_{LA}	T_{TA}	T_{ZA}
$20T_e/300$	0.77	297	358.1	329.6	343.2	318.1	321.2	321.7	304.7
$50T_e/300$	0.77	297	351.5	326.2	338.5	316.3	319.0	319.3	304.4
$20T_e/300$	0.77	448	492.4	481.9	486.2	477.1	480.9	480.8	468.5
$50T_e/300$	0.77	448	488.3	479.1	482.8	474.9	478.2	478.0	467.3
$20T_e/300$	0.77	523	567.3	560.4	563.3	556.6	559.8	559.7	549.5
$50T_e/300$	0.77	523	563.1	557.0	559.5	553.8	556.5	556.4	547.6
$20T_e/300$	0.77	598	643.7	638.9	641.1	635.8	638.5	638.4	630.2
$50T_e/300$	0.77	598	639.2	635.0	636.9	632.4	634.6	634.5	627.5
$20T_e/300$	*3.5*	297	484.1	434.1	454.4	402.2	423.8	423.3	339.2
$50T_e/300$	*3.5*	297	470.3	422.9	442.1	393.8	412.3	411.9	337.3
$20T_e/300$	**4.71**	297	530.0	478.0	499.4	442.8	470.4	469.6	359.2
$50T_e/300$	**4.71**	297	513.1	463.5	483.6	431.3	455.4	454.7	356.2

Table S2: Ratios of the Average ZA Phonon Temperature Rise Relative to the Temperature Rise of Other Energy Carriers in the Laser Spot

κ_e ($Wm^{-1}K^{-1}$)	Power (mW)	T_{stage} (K)	$\Delta T_{ZA}/\Delta T_e$	$\Delta T_{ZA}/\Delta T_{LO}$	$\Delta T_{ZA}/\Delta T_{TO}$	$\Delta T_{ZA}/\Delta T_{zo}$	$\Delta T_{ZA}/\Delta T_{LA}$	$\Delta T_{ZA}/\Delta T_{TA}$
$20T_e/300$	0.77	297	0.13	0.25	0.17	0.38	0.33	0.32
$50T_e/300$	0.77	297	0.14	0.26	0.19	0.39	0.34	0.34
$20T_e/300$	0.77	448	0.42	0.57	0.50	0.67	0.59	0.59
$50T_e/300$	0.77	448	0.44	0.58	0.51	0.68	0.60	0.60
$20T_e/300$	0.77	523	0.57	0.68	0.63	0.77	0.70	0.70
$50T_e/300$	0.77	523	0.58	0.70	0.64	0.78	0.71	0.71
$20T_e/300$	0.77	598	0.68	0.77	0.73	0.84	0.78	0.78
$50T_e/300$	0.77	598	0.69	0.78	0.74	0.84	0.79	0.79
$20T_e/300$	*3.5*	297	0.18	0.23	0.20	0.30	0.24	0.24
$50T_e/300$	*3.5*	297	0.19	0.25	0.22	0.33	0.26	0.26
$20T_e/300$	**4.71**	297	0.23	0.31	0.27	0.40	0.33	0.33
$50T_e/300$	**4.71**	297	0.23	0.32	0.28	0.42	0.35	0.35

4. Thermal conductivity extraction from Raman-based temperatures

The observed local nonequilibrium has been ignored in past heat diffusion analyses of Raman thermal transport measurements of graphene. To illustrate the effects of this assumption, we employ the analytic solution derived in a prior work[2] to extract the thermal conductivity of suspended graphene. For the calculation, we measured the amount of laser power absorbed by the graphene as 3.1 ± 1.4%, which was the difference between the measured transmittance through a 10 μm diameter hole covered by the suspended graphene and that through an uncovered hole of the same size. Based on the previously reported thermal conductivity and the interface thermal conductance of the supported graphene, we calculate that the thermal contact thermal resistance, $R_c \approx (1.6 + 1.5/-0.75)$ x 10^4 K/W, is small compared to the measured thermal resistance of the graphene, $R_m \approx (1.6 \pm 0.74)$ x 10^6 K/W, which is calculated as the measured graphene temperature rise by either a peak shift or the intensity ratio divided by the absorbed laser power. The thermal resistance of the suspended graphene is obtained as $R_g = R_m - R_c$, and used to calculate the thermal conductivity of the suspended graphene according to an analytical solution to the heat diffusion equation in the cylindrical coordinate.[2] The as-obtained apparent thermal conductivity depends on whether the optical phonon temperature or the peak shift-based temperature is used in this calculation. Figure 5 in the main text displays this apparent thermal conductivity versus the apparent graphene temperature, as measured at the highest laser power.

References

(1) Vallabhaneni, A. K.; Singh, D.; Bao, H.; Murthy, J.; Ruan, X. *Phys. Rev. B* **2016**, *93* (12), 125432.

(2) Cai, W.; Moore, A. L.; Zhu, Y.; Li, X.; Chen, S.; Shi, L.; Ruoff, R. S. *Nano Lett.* **2010**, *10* (5), 1645–1651.